energies

MDPI

Article

Optimization of Fuel Consumption and Emissions for Auxiliary Power Unit Based on Multi-Objective Optimization Model

Yongpeng Shen [1,*], Zhendong He [1], Dongqi Liu [2] and Binjie Xu [2]

[1] College of Electric and Information Engineering, Zhengzhou University of Light Industry, Zhengzhou 450002, China; hezhendong_itl@163.com

[2] College of Electric and Information Engineering, Hunan University, Changsha 4100822, China; liu.dongqi@hotmail.com (D.L.); xubinjie@hnu.edu.cn (B.X.)

* Correspondence: shenyongpeng@hnu.edu.cn; Tel.: +86-150-7317-3394; Fax: +86-371-6355-6790

Academic Editor: Omar Hegazy
Received: 14 September 2015; Accepted: 25 January 2016; Published: 2 February 2016

Abstract: Auxiliary power units (APUs) are widely used for electric power generation in various types of electric vehicles, improvements in fuel economy and emissions of these vehicles directly depend on the operating point of the APUs. In order to balance the conflicting goals of fuel consumption and emissions reduction in the process of operating point choice, the APU operating point optimization problem is formulated as a constrained multi-objective optimization problem (CMOP) firstly. The four competing objectives of this CMOP are fuel-electricity conversion cost, hydrocarbon (HC) emissions, carbon monoxide (CO) emissions and nitric oxide (NO_x) emissions. Then, the multi-objective particle swarm optimization (MOPSO) algorithm and weighted metric decision making method are employed to solve the APU operating point multi-objective optimization model. Finally, bench experiments under New European driving cycle (NEDC), Federal test procedure (FTP) and high way fuel economy test (HWFET) driving cycles show that, compared with the results of the traditional fuel consumption single-objective optimization approach, the proposed multi-objective optimization approach shows significant improvements in emissions performance, at the expense of a slight drop in fuel efficiency.

Keywords: electric vehicle; auxiliary power unit (APU); fuel consumption (FC); emissions; multi-objective optimization

1. Introduction

An auxiliary power unit (APU) is a device on a vehicle that provides electric energy to the drive system. APUs are widely used in various types of electric vehicles, such as series hybrid electric vehicles (SHEVs), range extended electric vehicles, and plug-in hybrid electric vehicles [1]. Improvements in fuel economy and emissions of these vehicles strongly depend on the supervisory control strategies. At a high hierarchical level, the supervisory control strategy determines the optimal power distribution between APU and power battery. At a lower hierarchical level, the one considered in this paper, the supervisory control strategy is responsible for operating the APU works on the the optimal region or point, where the fuel consumption and emissions are minimized simultaneously.

Focused on the optimization of life cycle CO_2 emissions and taxi owner's costs of Lisbon taxi fleet, Castel-Branco *et al.* [2] proposed a multi-objective genetic algorithm to achieve several trade-off optimal solutions for different driving patterns, and the results show that specifically optimized solutions could reduce in-use energy consumption by 43%–47% in urban driving, and 27%–34%

in extra-urban driving conditions, and reduce life cycle emissions by 47%–49% and 34%–36% respectively. Focused on the power distribution problem between the two power sources of the vehicle, Trovao *et al.* [3] proposed an integrated rule-based metaheuristic approach which determines the optimized real-time energy sharing between the two sources without prior knowledge of the power demand profile. The experimental results show that this approach is effective in controlling the two energy sources to work in their higher efficiency region and in satisfying the dynamic performance of the vehicle. Focused on the system integration and power-flow control of APU, Hu *et al.* [4] proposed an innovative multi-criteria optimization approach and showcases its validity and usefulness in a bus. In order to analyze and optimize the power flow between the APU and battery of plug-in hybrid electric vehicle, Mapelli *et al.* [5] developed an energetic model. The control method, driving mode and inverter losses of the vehicle power train were analyzed based on this model. He and Yang [6] proposed a robust linear parameter-varying (LPV) method which attempts to optimize the APU fuel efficiency through stabilize the APU working point at the maximum efficiency region. Gokasan *et al.* [7] proposed a novel approach in the optimization of APU fuel efficiency. Two chattering-free sliding-mode controllers (SMCs) were developed to keep the engine operating in the optimal efficiency region. One of the SMCs adjusts the engine throttle to maintain the engine speed at a certain level, while the other performs engine/generator torque control via the power converter, so that the engine works in the optimal efficiency region, despite load variations. For more details about different approaches in improving fuel efficiency and emissions of vehicles with APU, see [8–14].

One of the general characteristics of the aforementioned approaches is that they attempt to optimize the fuel efficiency and emissions simultaneously just based on the speed-torque/power-fuel efficiency characteristics of the internal combustion engine (ICE). However, on the speed-torque map of an ICE, the locus of maximum fuel efficiency does not necessarily correspond to the loci of optimum emissions. In some cases, they are even two sections in the map of optimum performance [15]. In other words, the operating point with minimum fuel consumption (FC) does not necessarily result in the minimum emissions. The challenge for the APU operating point optimization problem is how to balance the goals of higher fuel efficiency and lower emissions simultaneously.

Unlike the aforementioned control strategies that employ the isolated speed-torque/power FC map and show little sensitivity to subtle emissions tradeoffs in the choice of APU operating points, the main contribution of this paper is to ensure that the APU operates on the multi-objective optimal points. To achieve this goal and balance the conflicting goals of FC and emissions reduction in the choice of operating point, the APU operating point optimization problem is formulated as a constrained multi-objective optimization problem (MOP) with competing objectives of fuel-electricity conversion (FE) cost, hydrocarbon (HC) emissions, CO emissions and NO_x emissions.

The rest of this paper is organized as follows. In Section 2, the APU operating point multi-objective optimization model (MOM) is formulated. In Section 3, the multi-objective particle swarm optimization (MOPSO) algorithm and weighted metric decision making method which are employed to solve the MOM are introduced briefly. In Section 4, the off-line optimization of the MOM is performed. In Section 5, bench experiments are carried out over three typical driving cycles, and comparisons are made between the results of the proposed approach and that of the traditional single-objective approach (SOA). The conclusion is presented in Section 6.

2. Auxiliary Power Unit Operating Point Multi-objective Optimization Model

2.1. Features of the Auxiliary Power Units

The APU scheme considered in this paper is suitable for SHEVs and consists of a generator and an ICE, a common shaft connects the ICE and generator directly, as shown in Figure 1. The vehicle is driven by a traction motor, and the traction motor is powered by the battery and/or APU through a motor controller. The powers of both power sources are merged together in a controllable electrical

coupling device, thus the APU is mechanically decoupled from the driven wheels. In the start-up phase, the generator acts as a starting motor, while in the other working phase, it acts as a battery charger. The APU control unit determines the operating point of the APU $(n_{\text{cmd}}, T_{\text{cmd}})$ according to the power demands instruction P_{cmd} from vehicle control unit, where n_{cmd} and T_{cmd} are the engine speed and generator torque commands, respectively. P_{cmd} is the expected APU power of the vehicle control unit, and it is dependent on the vehicle control strategy, vehicle parameters, driving cycles as well as the realtime regenerative braking power. At the same time, the real-time APU working information, such as APU rotational speed n, APU output voltage V_{apu} and current I_{apu} are input parameters of the APU control unit.

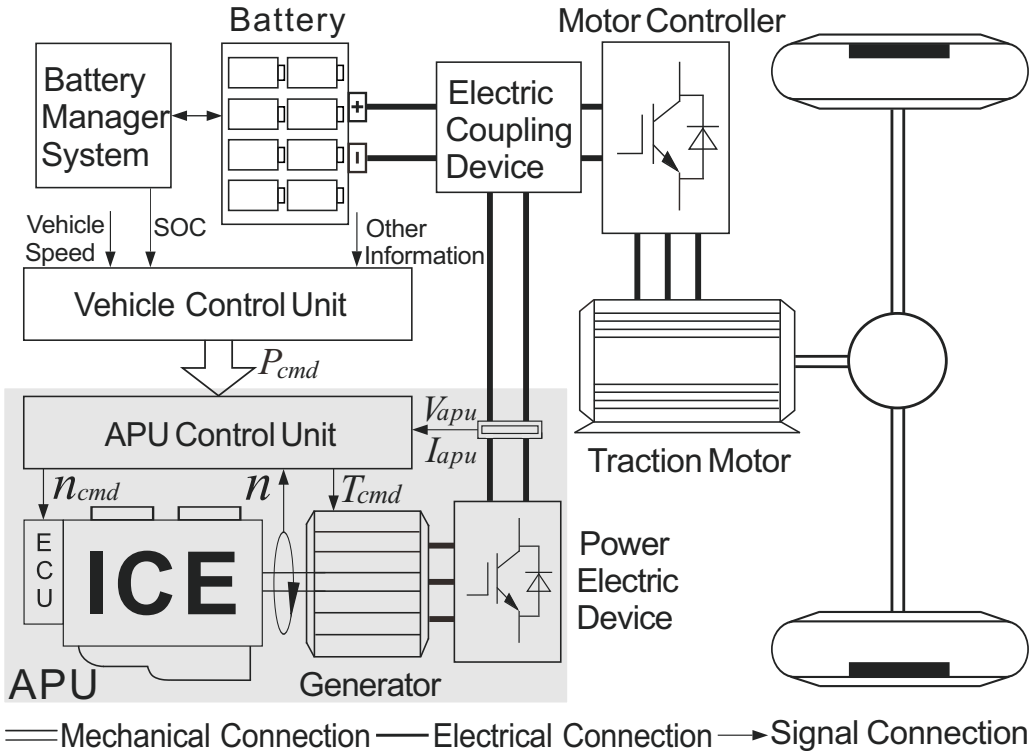

Figure 1. Schematic of the auxiliary power unit (APU) and its application in series hybrid electric vehicle (SHEV). Internal combustion engine: ICE.

The fuel efficiency and emissions of the APU are directly dependent of its operating points on the speed-torque/power-fuel efficiency characteristics map and speed-torque/power-emissions characteristics maps of the ICE [16]. Furthermore, due to the mechanical decoupling of the APU from the driven wheels, the speed and torque of the engine are independent of vehicle speed and traction torque demand, and can be controlled to any operating point on its speed-torque plane. Consequently, the APU should be controlled in such a way that it always operates in its optimal operation region, where FC, HC, CO and NO_x emissions of the APU are minimized simultaneously. However, due to the inherent characteristics of the ICE, the FC and fuel emissions are unable to reach their minimum values at same operating point. In other words, on the speed-torque/power map of an ICE, the locus of maximum fuel efficiency does not necessarily correspond to the loci of optimum emissions and their is a definite tradeoff between high fuel efficiency and low emissions. Figure 2 shows a schematic of desired operating locations of a spark ignition (SI) engine.

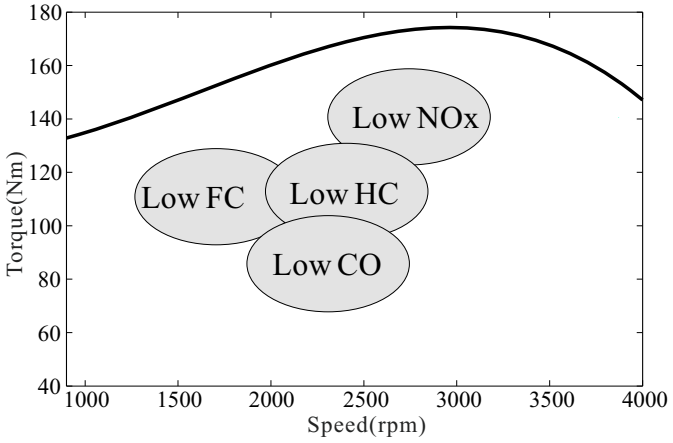

Figure 2. Fuel efficiency and emissions tradeoffs for an spark ignition (SI) engine.

2.2. Optimization Objectives

The speed-torque-fuel consumption characteristics $f_{\mathrm{FC}}(n,T)$, HC emissions characteristics $f_{\mathrm{HC}}(n,T)$, CO emissions characteristics $f_{\mathrm{CO}}(n,T)$ and NO_x emissions characteristics $f_{\mathrm{NO}_x}(n,T)$ of a 42 kW gasoline engine are shown in Figure 3a–d, respectively. These engine speed-torque characteristics are all derived from engine bench experiments. Obviously, the operating point with minimum FC does not results in minimum emissions, and there is a definite tradeoff among FC, HC, CO and NO_x emissions. Thus, it is essential to balance the competing goals of higher fuel efficiency and lower emissions with multi-objective optimization approach.

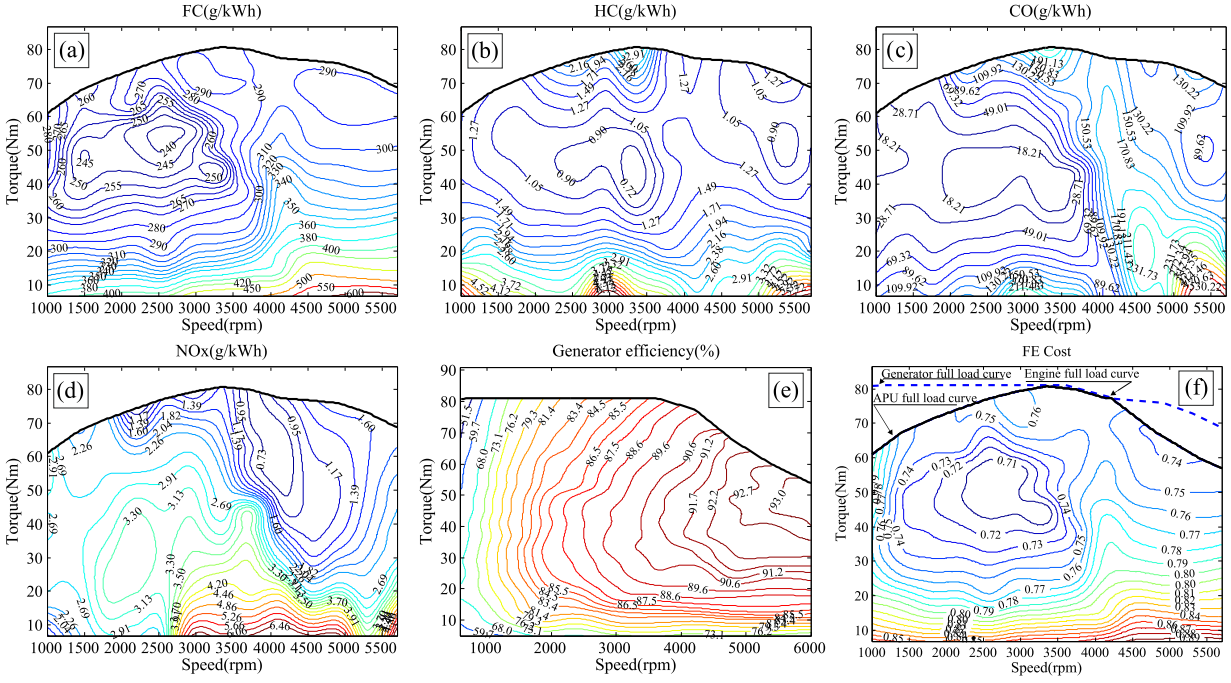

Figure 3. Speed-torque characteristics of the APU. (**a**) Fuel consumption (FC); (**b**) hydrocarbon (HC) emissions; (**c**) CO emissions; (**d**) NO_x emissions; (**e**) generator efficiency; and (**f**) fuel-electricity conversion (FE) cost.

Since the FC characteristics $f_{\mathrm{FC}}(n,T)$ denote the engine conversion efficiency from fuel to mechanical power while the considered APU output is electric power, the generator efficiency must

be taken into account. Here, the APU conversion efficiency from fuel to electricity is introduced by the following equation and is referred to as FE efficiency characteristics $f_{\mathrm{FE}}(n,T)$,

$$f_{\mathrm{FE}}(n,T) = \frac{360 \cdot f_{\mathrm{GE}}(n,T)}{f_{\mathrm{FC}}(n,T) \cdot Q_{\mathrm{HV}}} \tag{1}$$

where, $f_{\mathrm{GE}}(n,T)$ is the generator efficiency characteristics, as shown in Figure 3e, which is derived from the bench test data of a 35 kW permanent magnet synchronous motor (PMSM). Q_{HV} is the heating value of gasoline (4.6×10^7 J/kg).

For the HC, CO and NO_x emissions, smaller $f_{\mathrm{HC}}(n,T)$, $f_{\mathrm{CO}}(n,T)$ and $f_{\mathrm{NO}_x}(n,T)$ are expected, that is they are minimization problems. However, for the FE efficiency, larger $f_{\mathrm{FE}}(n,T)$ is expected and it is a maximization problem. In order to formulate a uniform minimization problem, the APU FE cost characteristics are introduced by the following equation:

$$f_{\mathrm{cost}}(n,T) = 1 - f_{\mathrm{FE}}(n,T) \tag{2}$$

The resulted APU FE cost map is shown in Figure 3f. The FE cost is essentially the energy loss ratio in the process of FE. One other thing to note is that the full load characteristics of the APU are determined by the full load characteristics of both engine and generator. Thus the feasible operating area of the APU is the intersection area of the engine full load curve and generator full load curve, as shown in Figure 3f.

Based on the above analysis, the APU operating point optimization problem can be formulated as a multi-objective optimization problem which contains two independent variables (n,T) and four competing objectives FE cost, HC emissions, CO emissions and NO_x emissions,

$$\text{minimize}: \quad F(n,T) = [f_{\mathrm{cost}}(n,T), f_{\mathrm{HC}}(n,T), f_{\mathrm{CO}}(n,T), f_{\mathrm{NO}_x}(n,T)] \tag{3}$$

2.3. Constraints

In the real-world APU operating point optimization problems, the feasible APU operating area is subjected to the constraints imposed by APU full load characteristics and the power demands of the vehicle control unit.

On one hand, the full load characteristics of the APU are determined by the full load characteristics of both engine and generator, as shown in Figure 3f. The APU minimum operating torque T_{min} is the larger one between the engine minimum operating torque Te_{min} and the generator minimum operating torque Tg_{min}. The APU maximum operating torque T_{max} is a function of APU rotational speed n and is determined by the full load characteristics of both engine and generator, as described in Equation (4):

$$\begin{cases} T_{\mathrm{min}} = \max(Te_{\mathrm{min}}, Tg_{\mathrm{min}}) \\ T_{\mathrm{max}} = f_{\mathrm{tm}}(n) = \min(Te_{\mathrm{max}}(n), Tg_{\mathrm{max}}(n)) \end{cases} \tag{4}$$

where $Te_{\mathrm{max}}(\mathrm{n})$ and $Tg_{\mathrm{max}}(\mathrm{n})$ are the full load characteristics of engine and generator, respectively. Furthermore, the minimum and maximum allowable APU rotational speed are determined by the minimum and maximum allowable rotational speed of both engine and generator, as described in Equation (5):

$$\begin{cases} n_{\mathrm{min}} = \max(ne_{\mathrm{min}}, ng_{\mathrm{min}}) \\ n_{\mathrm{max}} = \min(ne_{\mathrm{max}}, ng_{\mathrm{max}}) \end{cases} \tag{5}$$

where $n_{\min}$ and $n_{\max}$ are the minimum and maximum allowable APU rotational speed, respectively. $ne_{\min}$ and $ne_{\max}$ are the minimum and maximum allowable engine rotational speed, respectively. $ng_{\min}$ and $ng_{\max}$ are the minimum and maximum allowable generator rotational speed, respectively.

On the other hand, according to the format of the power demands P_{cmd} of the vehicle control unit, the constraints imposed on the APU operating point (n, T) can be classified into three main categories: (1) finding the global optimal operating point in the whole map regardless of the APU output power; (2) finding the optimal operating point while guaranteeing the APU output power is in a specific power interval; (3) finding the optimal operating point while guaranteeing the expected APU output power.

(1) Global optimization [17,18], that is $P_{\text{cmd}} \in \mathbb{R}$, where $\mathbb{R}$ means all the feasible operating area of the APU. In this case, the APU can be operated on any operating points and the independent variables (n, T) must fulfill the following equation:

$$\begin{cases} n_{\min} \leq n \leq n_{\max} \\ T_{\min} \leq T \leq f_{\text{tm}}(n) \end{cases} \tag{6}$$

where $f_{\text{tm}}(n)$ is the APU maximum operating torque which defined by Equation (4).

(2) A specific power interval [19], that is $P_{\text{cmd}} \in [P_{\text{low}}, P_{\text{high}}]$. In this case, the feasible APU operating area is restricted to a certain power interval and the constraints are described as:

$$\begin{cases} \max(n_{\min}, \Xi_x(f_{\text{tm}}(n), g(P_{\text{low}}, n))) \leq n \leq \min(n_{\max}, \Xi_x(T_{\min}, g(P_{\text{high}}, n))) \\ \max(T_{\min}, g(P_{\text{low}}, n)) \leq T \leq \min(f_{\text{tm}}(n), g(P_{\text{high}}, n)) \end{cases} \tag{7}$$

where $\Xi_x(f_{\text{tm}}(n), g(P_{\text{low}}, n))$ is the x coordinate of the intersection point of $f_{\text{tm}}(n)$ and $g(P_{\text{low}}, n)$, $g(P, n)$ is a formula that describes the relation between torque and speed when power is P:

$$g(P, n) = \frac{30 \cdot P}{\pi n} \tag{8}$$

As an example, the feasible operating area of the APU when $P_{\text{cmd}} \in [5, 25]$ is shown in Figure 4. The 10 kW, 15 kW and 20 kW power isolines are also shown in Figure 4.

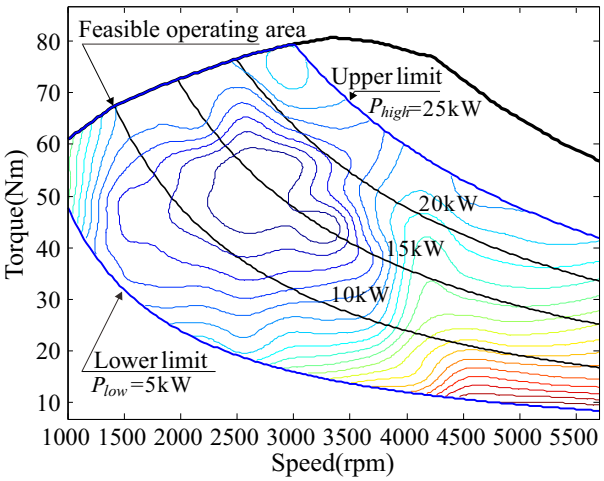

Figure 4. Feasible operating area when $P_{\text{cmd}} \in [5, 25]$.

(3) A specific power value [7,20], that is $P_{\text{cmd}} = P_{\text{set}}$. In this case, the independent variables (n, T) are located on the power isoline P_{set} and must fulfill the following equation:

$$\begin{cases} \max(n_{\min}, \Xi_x(f_{\text{tm}}(n), g(P,n))) \le n \le \min(n_{\max}, \Xi_x(T_{\min}, g(P,n))) \\ T = g(P,n) \end{cases} \tag{9}$$

According to the above analysis, we know that the APU operating point optimization MOM is a constrained multi-objective optimization problem (CMOP) which aims to minimize the four objective functions shown in Equation (3) and is subjected to the constraints imposed by Equations (6) and (7) or Equation (9).

3. Solving the Auxiliary Power Units Operating Point Multi-Objective Optimization Model

3.1. Multi-Objective Optimization

Like the considered APU operating point optimization problem, many real-world applications involve simultaneous optimization of multiple objectives which are often conflicting with each other and subject to a number of equality or inequality constraints [21–26]. In general, a CMOP can be formulated as follows:

$$\begin{aligned} &\text{minimize}: \ [f_1(\boldsymbol{x}), f_2(\boldsymbol{x}), \cdots, f_k(\boldsymbol{x})] \\ &\text{subject to}: \ g(\boldsymbol{x}) \le 0 \end{aligned} \tag{10}$$

where k is the number of objective functions, $f_i : \mathbb{R}^s \longrightarrow \mathbb{R}$, $\boldsymbol{x} = [x_1, x_2, \cdots, x_s]^T$ is the vector of independent variables.

Different from the single objective optimization problem (SOP) in which one or several global optimal solutions are available, in MOP, it is usually not possible to find a single solution that would be optimal for all objective functions simultaneously due to the contradiction and possible incommensurability of the objective functions. The optimal solutions for MOP are usually referred to "Pareto optimal set" or "Pareto set" [27]. The Pareto set of an MOP is usually an infinite set or a discrete approximation which contains large amounts of individual solutions. However, from the practical standpoint, users usually need only one solution which finally acts on the optimization object, and thus it is essential to choose one best compromise solution out of the Pareto set by a specific decision making method.

Based on the above analysis, the process of solving an MOP can be divided into two steps:

(1) Obtain the Pareto set or the well-distributed discrete approximation of the Pareto set of the MOP by a specific multi-objective optimization approach;
(2) Choose one best compromise solution out of the Pareto set by a decision making method.

3.2. Multi-Objective Particle Swarm Optimization

In engineering and scientific research, evolutionary algorithms are effective methods for calculating the Pareto set of an MOP, such as SPEA (strength Pareto evolutionary algorithm) [28], NSGA-II (non-dominated sorting genetic algorithm II) [29], MOPSO [30] and MOEA/D (multi-objective evolution algorithm based on decomposition) [31]. Here, the MOPSO is employed to solve the APU operating point MOM, because of its high searching ability and low time complexity (for the MOP to be solved, the MOPSO requires less computing time than that of the NSGA-II, microGA and PAES algorithms) [30].

As a variant of the basic particle swarm optimization algorithm (PSO), the MOPSO inherits the basic concepts of the PSO, such as velocity and position update. The MOPSO adopts an external elitist archive (EA) to store the non-dominated solutions that are found during the evolutionary process, and the adaptive grids mechanism is utilized to improve the diversity of the resulted Pareto solutions.

The pseudo code of the MOPSO is presented in Algorithm 1, where the overall computational flow is described, and the EA update rules, adaptive grids mechanism, velocity and position update rules are described in detailed (highlighted in bold italic fonts).

Algorithm 1: MOPSO (k, s, N, $E_{\max}$, d, μ, τ_1, τ_2, $t_{\max}$)

k, number of the objective functions;
s, number of the independent variables;
N, population size;
$E_{\max}$, *maximum size of EA;*
d, number of grids in each dimension of the objective space;
μ, *inertia weight*, $\mu \in [0,1]$;
τ_1, *acceleration coefficient 1;*
τ_2, *acceleration coefficient 2;*
$t_{\max}$, *maximum iteration number.*

Initialization: $p[i][j] = rand$, $t = 0$, v_j^i=0, EA=$\varnothing$, i=$(1, 2, \cdots, N)$, j=$(1, 2, \cdots, s)$
while $t \leq t_{\max}$ **do**
  for $i = 1$ to N **do**
    External archive update rules:
    if $P^i \succ \forall\, EA[\lambda]$ **then**
      Update EA: $EA \leftarrow EA \cap \overline{EA}[\tau] \cup P^i$, τ is the dominated individual
    else if $(P^i \not\succ \forall\, EA[\lambda]) \wedge (P^i \not\prec \forall\, EA[\lambda])$ **then**
      Update EA: $EA \leftarrow EA \cup P^i$
    end if
    if $|EA| > E_{\max}$ **then**
      Adaptive grids mechanism:
      if $f_j(P^i) \in [\min_j, \max_j]$, $j \in (1, 2, \cdots, k)$ **then**
        $EA \leftarrow EA \cap \overline{EA}[\xi]$, ξ is the removed particle
      else
        Grids redivide, and $EA \leftarrow EA \cap \overline{EA}[\xi]$
      end if
    end if
    Individual best position Pb^i update
  end for
  Global best position P_g update
  for $i = 1$ to N **do**
    for $j = 1$ to s **do**
      Velocity and position update:
      $v_j^i = \mu \cdot v_j^i + \tau_1 r_1 [pb_j^i - p_j^i] + \tau_2 r_2 [pg_j - p_j^i]$
      $p_j^i = p_j^i + v_j^i$
    end for
  end for
  t=t+1
end while
Output the Pareto optimal set EA

3.3. Multi-Objective Decision Making

The second issue of solving an MOP is finding out a *best compromise solution* from the Pareto set. To address this issue, different approaches have been proposed, such as fuzzy group decision making method [32], rough set decision making method [33] and weighted metric decision making method [34,35]. Here, the weighted metric decision making method is employed to choose one best compromise solution out of the Pareto set obtained by MOPSO.

Since the four objectives of the proposed MOM are in different units and scales, they should be converted to a similar nondimensional scale before applying the weighted metric decision making method. To facilitate this, each of the four metrics is normalized to a value between 0 and 1 by the following equation:

$$\overline{f}_{ij}(\boldsymbol{x}) = \frac{f_{ij}(\boldsymbol{x}) - f_j^m}{f_j^M - f_j^m}, \quad j = 1, 2, \cdots, k \tag{11}$$

where $f_j^m = \min_{i=1,\cdots,E_{\max}} f_{ij}(\boldsymbol{x})$, $f_j^M = \max_{i=1,\cdots,E_{\max}} f_{ij}(\boldsymbol{x})$.

According to the weighted metric method, the weighted metric of each Pareto optimal solution is calculated according to the following equation:

$$l_i(x) = \sqrt{\sum_{m=1}^{4} \omega_m |\overline{f}_{im}(x) - z_m^*|^2} \tag{12}$$

where m= (1, 2, 3, 4), $i = (1, 2, \cdots, E_{\max})$, ω_m is the weighting factor of each objective function, z_m^* is the expected solution of the MOM. Here, $z_m^* = 0$, since the MOM is a minimization optimization problem. The Pareto optimal solutions which gives the smallest weighted metric value is selected as the best compromise solution.

4. Off-Line Optimization

According to the APU FE cost and emissions characteristics shown in Figure 3b–d,f the off-line optimization of the MOM is performed. Firstly, the MOPSO is performed to calculate the Pareto optimal set of the APU operating point MOM. Then, the weighted metric method is utilized to obtain the best compromise solution.

The parameters of the MOPSO are set as population size N = 200, EA size $E_{\max}$ = 200, grids number d = 4, inertia weight μ = 0.4, acceleration coefficients τ_1 = 2.0, τ_2 = 2.0, maximum iteration number $t_{\max}$ = 80.

4.1. Global Optimization

In the global optimization mode, the distribution of the resulted Pareto set is illustrated in Figure 5, the FE cost characteristics are also shown in Figure 5. The best compromise solution when weighting factors are set as W = (0.4, 0.2, 0.1, 0.3) is marked with "○" in Figure 5. Here, W = (0.4, 0.2, 0.1, 0.3) is a typical combination which can reflect the relative importance of the four optimization objectives. A feasible guideline for weighting factors selection is that preset the weighting factors according to the local emission standards. Due to the fact that different countries have different emission regulations, and these regulations are becoming more and more stringent, it is essential to set different combinations of the weighting factors to meet the local emission standards.

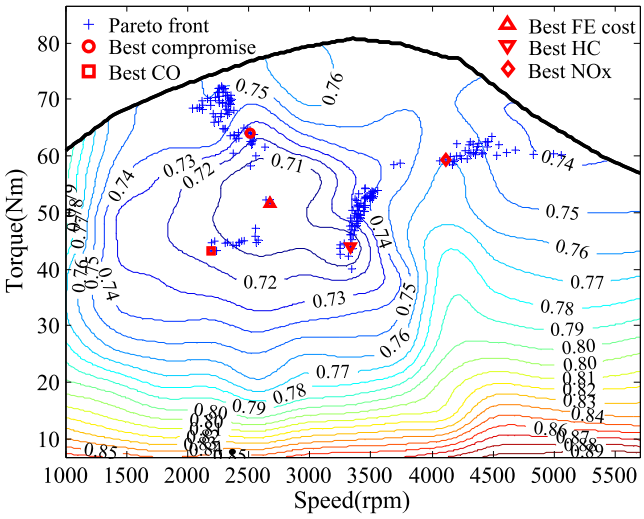

Figure 5. Distribution of the Pareto set.

As shown in Figure 5, the APU operating point with best FE cost is (n, T) = (2813.07, 55.26), where the FE cost is $f_{\mathrm{FE}}(n, T) = 0.6992$; The APU operating point with best HC emissions is (n, T) = (3329.01, 44.02), where the HC emissions are $f_{\mathrm{HC}}(n, T) = 0.6057$ g/kWh; The APU operating point with best CO emissions is (n, T) = (2188.80,43.25), where the CO emissions are $f_{\mathrm{CO}}(n, T) = 9.5618$ g/kWh; The APU operating point with best NO_x emissions is $(n, T) = (4108.67, 59.38)$, where the NO_x emissions are $f_{\mathrm{NO}_x}(n, T) = 0.5162$ g/kWh; The best compromise APU operating point is $(n, T) = (2508.47, 64.08)$, where the objective values are $F(n, T) = [0.7231, 1.3758, 59.6303, 2.2970]$. The distribution of the Pareto front is illustrated in four three-dimensional diagrams and each of them shows the distribution of the Pareto front among three different objectives, as shown in Figure 6. The best compromise APU operating point and the APU operating points with best HC, CO and NO_x emissions are also marked in Figure 6.

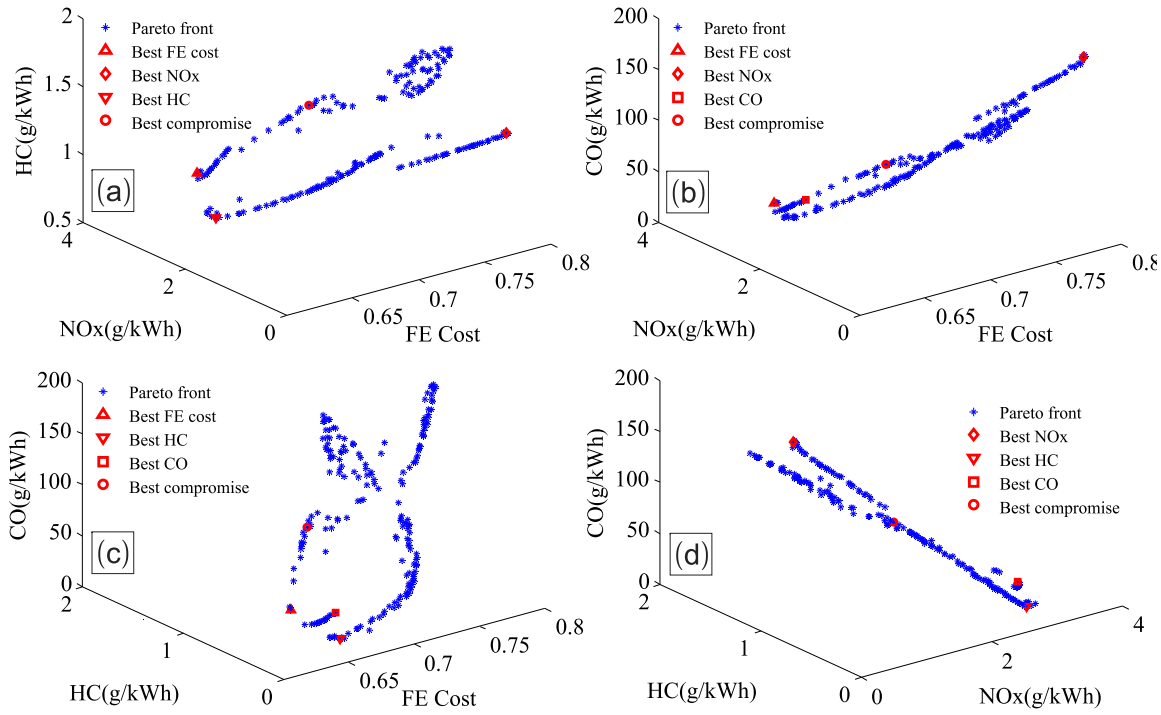

Figure 6. Distribution of the Pareto front. (**a**) Pareto front in FE cost-NO_x-HC space; (**b**) Pareto front in FE cost-NO_x-CO space; (**c**) Pareto front in FE cost-HC-CO space; and (**d**) Pareto front in NO_x-HC-CO space.

4.2. Specific Power Optimization

If the global optimization of the MOM is performed, it gives the global optimal solution (n, T). The APU will produce balanced optimal FE cost, HC, CO and NO_x emissions if it works on this point. However, the APU output power is constant if its operating point is fixed. In most cases, the APU output power must be adjusted with the demands of the high-level vehicle control strategy, such as power following charge depleting (PFCD) strategy. In order to produce multi-objective operating point for specific power demands, the MOPSO and weighted metric method are performed at different P_{cmd} between 1 kW and 34 kW with power interval of 1 kW, and then 34 multi-objective operating points are obtained. The multi-objective optimal trajectory is defined by these points. For different P_{cmd} of the high-level vehicle control strategy, the engine speed and torque adjusted according to the multi-objective optimal trajectory.

The resulted best compromise APU operating points and the multi-objective optimal trajectory when W = (0.4, 0.2, 0.1, 0.3) are shown in Figure 7. As a comparison, the brake specific FC (BSFC) optimal trajectory is also shown in Figure 7.

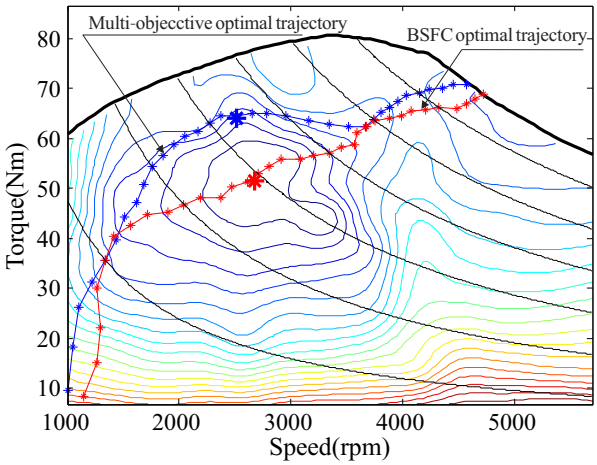

Figure 7. Multi-objective optimal trajectory and the brake specific FC (BSFC) optimal trajectory.

The BSFC optimal trajectory is the optimal result of FC which does not considers the potential HC, CO and NO_x tradeoffs. The BSFC optimal operating points are the optimal results of FC single-objective optimization. In the experiments, both of multi-objective optimal trajectory and BSFC optimal trajectory are utilized, and comparisons are made between their results.

5. Bench Experiment and Results Analysis

5.1. Experimental Facility and Process

In order to validate the effects of the resulted multi-objective optimal trajectory on the final vehicle FC and emissions, bench experiments are carried out based on AVL (a trade mark) puma open test system. The schematic diagram and photo of the experimental bench are shown in Figure 8a,b, respectively. The function of each component of the experimental bench is described as below:

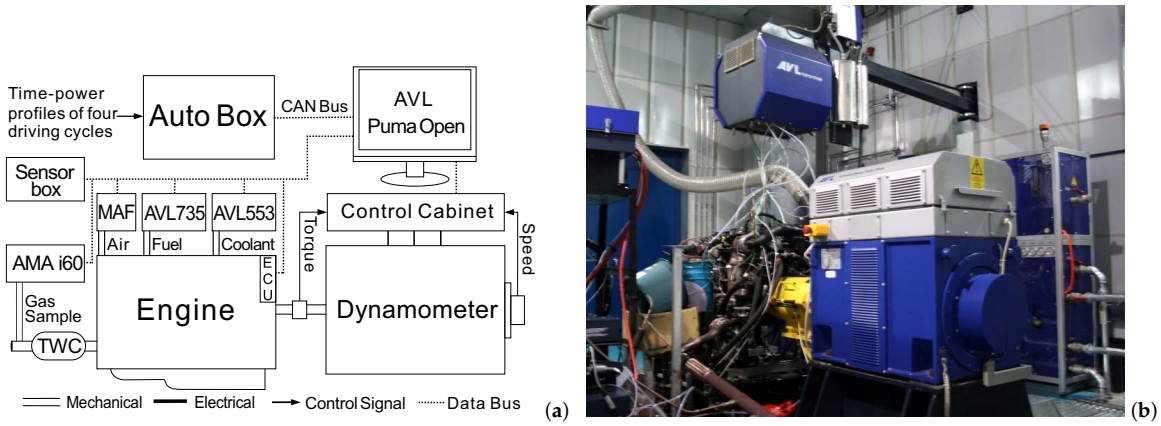

Figure 8. Schematic diagram and photo of the experimental bench. (**a**) Schematic diagram of the experimental bench; and (**b**) photo of the experimental bench.

(1) Autobox: A rapid control prototyping toolkit. It is a real-time controller with real I/O interfaces. Here, it acts as an APU control unit;
(2) AVL puma open: A test bench automation system. It offers an integrated solution for data acquisition and experiment procedure management. Here, it receives speed/torque (n, t) command from the AutoBox through controller area network (CAN) bus and manipulates the

dynamometer/engine works in "T/N" mode (defined by AVL, it means that the dynamometer works in torque control mode and engine works in speed control mode);
(3) Dynamometer: An AC electric dynamometer. Here, it serves as a controllable load of the engine.
(4) Control cabinet: An electric device that is used to drive the electric dynamometer according to the torque command of the AVL puma open;
(5) AVL 735: Fuel mass flow meter. It reports the FC of the engine;
(6) AVL 553: Coolant temperature regulating system. It is used to regulate the coolant temperature to 20 °C before each driving cycle;
(7) AMA i60 (a trade mark): Exhaust analysis device. It reports the HC, CO and NO_x emissions of the engine;
(8) mass flow meter (MAF): Air mass flow meter. It reports the engine intake air mass flow rate, which is a parameter used in exhaust emission data processing;
(9) Sensor box: A integrated sensor signal process unit. Here, it used to collect sensor signals such as temperature and humidity of the engine intake air;
(10) TWC: Three-way catalytic converter. It is a engine emissions after-treatment devices that converts toxic HC, CO and NO_x emissions to less toxic pollutants.

The three typical driving cycles used in the experiment are New European driving cycle (NEDC), Federal test procedure (FTP) and High way fuel economy test (HWFET). The PFCD strategy is utilized as the high-level vehicle control strategy [16]. Before the bench experiments, the power demands P_{cmd} of NEDC, FTP, and HWFET driving cycles are calculated according to the vehicle dynamics [16], PFCD and vehicle parameters shown in Table 1, the required total power curves for the three driving cycles are shown in Figures 9a–11a, respectively. The vehicle speed curves and the resulted APU power curves for three driving cycles are shown in Figures 9b–11b, respectively. For the three driving cycles, the battery power, battery voltage, battery current and SoC curves are shown in Figures 12 and 13, respectively. In the above process, the "fixed speed-ratios between electric and mechanical braking forces" regenerative braking control strategy is employed, that is for a specific total braking torque required and a specific vehicle speed, the vehicle control unit calculates the distribution of the braking forces between the electric and mechanical braking torque according to the predefined ratio [16]. The regenerative braking power is controlled by the vehicle unit and charged to the batteries and reused in later propelling. As an important part of the higher high-level vehicle control strategy, the regenerative braking power is eventually reflected in the changes in the power demands P_{cmd}. For each driving cycle, the corresponding time-power profile serves as the load signal P_{cmd} of the APU, and the load operation is eventually performed by the electric dynamometer.

Table 1. Vehicle parameters used in power computation. Permanent magnet synchronous motor: PMSM.

Components	Parameters	Values
Engine	Engine displacement (L)/Peak power (kW) Min/max speed (rpm)	1.0/42 998/5700
Generator	Type Rated power (kW)/max speed (rpm)	PMSM 32/6000
Power battery	Type/max continuous discharge current (C) Nominal voltage (V)/Capacity (Ah)	LiFePO/2C 330/10
Driving motor	Type Peak power (kW)/max speed (rpm)	IM 75/9000
Others	Front area (m^2) Aerodynamic drag coefficient Rolling resistance coefficient Wheel radius (r/m) Wheel base/wheel tread (mm) Vehicle mass/gross mass (kg)	1.835 0.28 0.009 0.305 2600/1470 1006/1242

Here the proposed multi-objective approach (MOA) is compared with the traditional SOA. For the SOA, it shares the same experimental facility and process with the MOA, except that it calculates the APU operating point (n, T) according to the BSFC optimal trajectory shown in Figure 7. For the SOA, the PSO algorithm is utilized, and the parameters of the PSO are set as inertia weight $\mu = 0.4$, acceleration coefficients $\tau_1 = 2.0$, $\tau_2 = 2.0$, population size $N = 200$ and maximum iteration number $t_{max} = 80$.

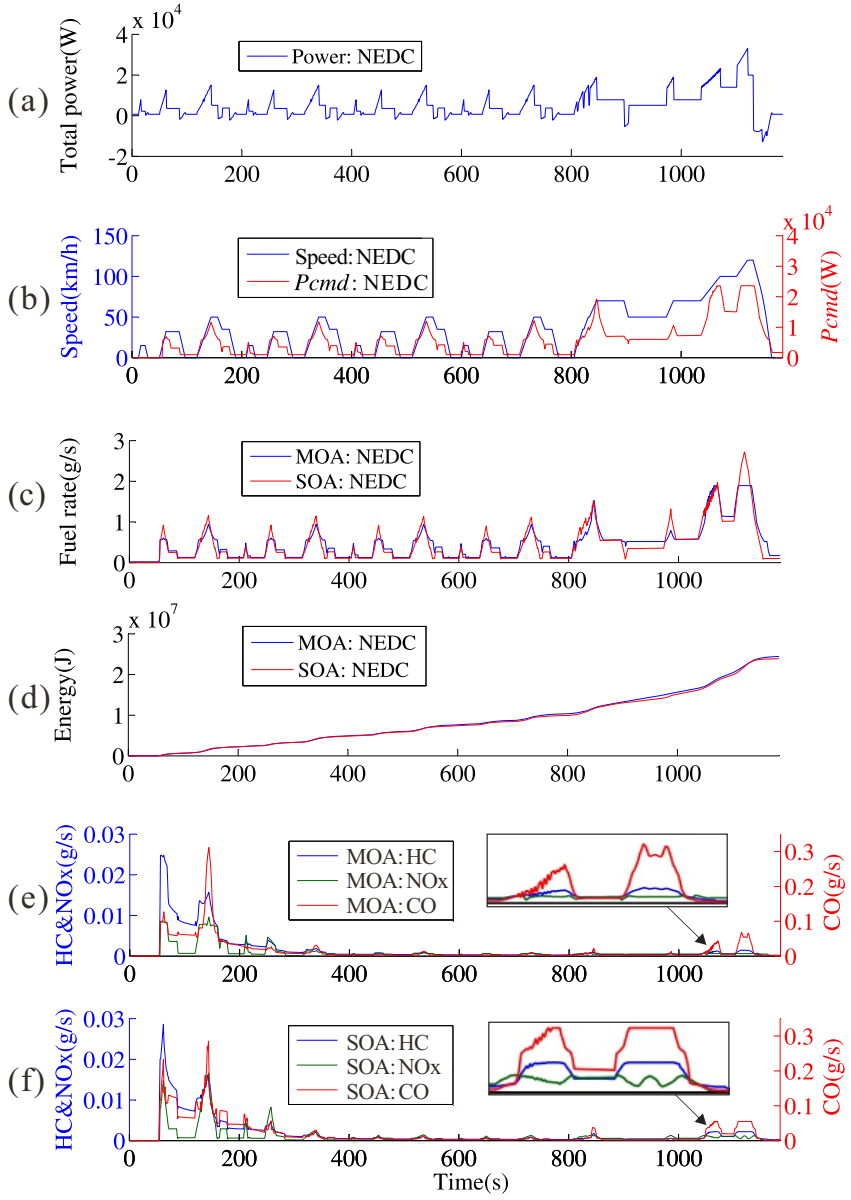

Figure 9. Required total power, speed, power, fuel rate, cumulative energy consumption and emissions of the New European driving cycle (NEDC) driving cycle. (**a**) total power; (**b**) speed and power; (**c**) fuel rate; (**d**) cumulative energy consumption; (**e**) emissions from MOA; and (**f**) emissions from single-objective approach (SOA).

For each driving cycle, the experiment process is described as follows:

(1) Regulate the coolant temperature to 20 °C by AVL 553 and regulate the the TWC temperature to 20 °C through natural cooling;

(2) The AutoBox determines the APU operating point (n, T) according to the time-power profile and the multi-objective optimal trajectory (if the proposed MOA is performed) or the BSFC optimal trajectory (if the SOA is performed). The resulted APU operating point (n, T) is send to AVL Puma Open through CAN bus. If the expected APU power is less than 5 kW, then the engine speed and dynamometer torque are set to idle speed and 0 Nm, respectively, that is $(n, T) = (998, 0)$;

(3) Set the experimental bench to "T/N" mode and adjust the engine speed and dynamometer torque to n and T, respectively;

(4) Goto step 2.

Step 2 to step 4 are repeated at a frequency of 1 HZ until the end of the driving cycle.

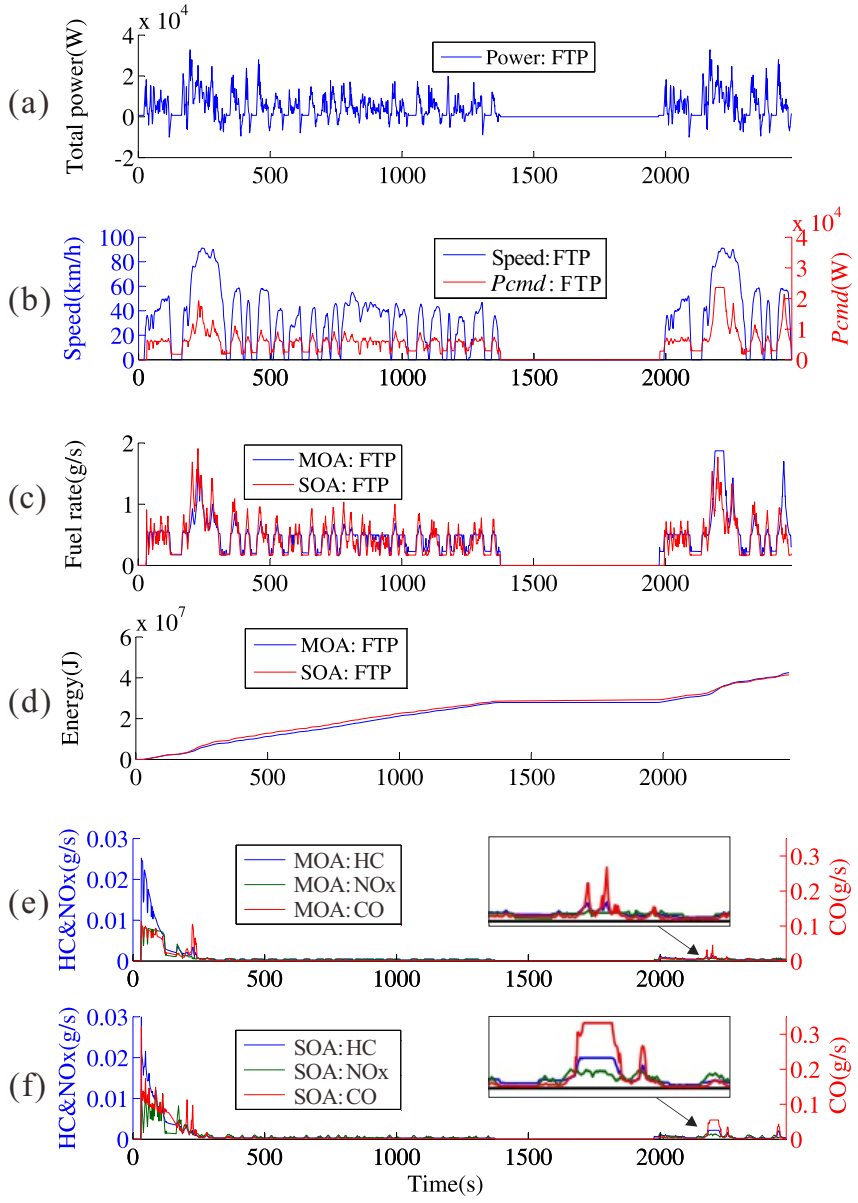

Figure 10. Required total power, speed, power, fuel rate, cumulative energy consumption and emissions of the Federal test procedure (FTP) driving cycle. (**a**) total power; (**b**) speed and power; (**c**) fuel rate; (**d**) cumulative energy consumption; (**e**) emissions from MOA; and (**f**) emissions from SOA.

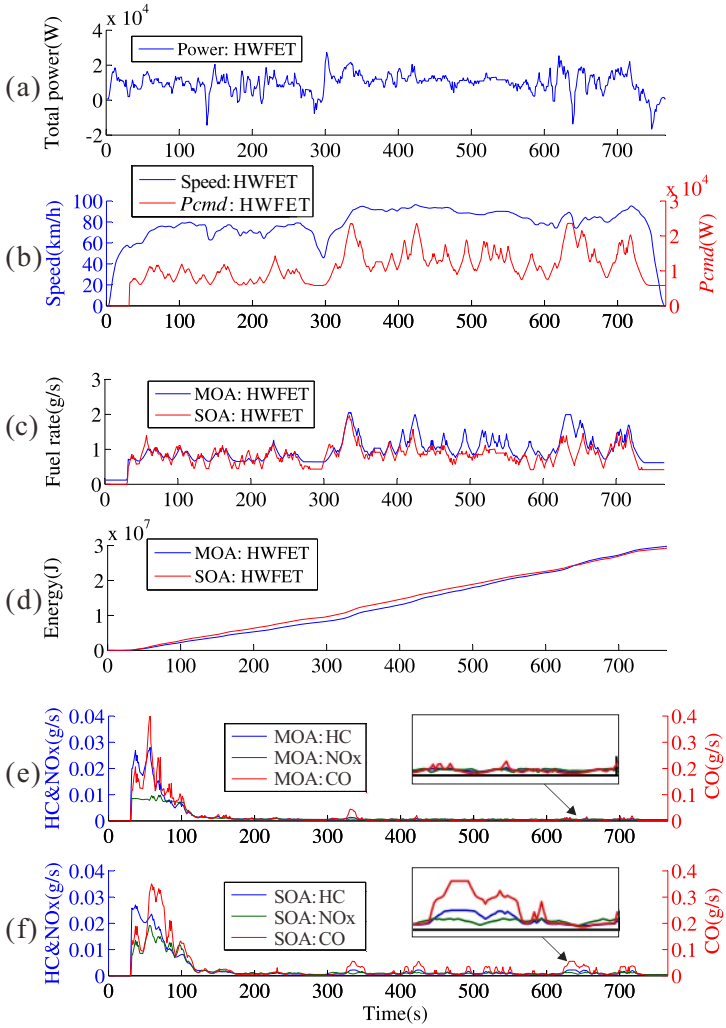

Figure 11. Required total power, speed, power, fuel rate, cumulative energy consumption and emissions of the high way fuel economy test (HWFET) driving cycle. (**a**) total power; (**b**) speed and power; (**c**) fuel rate; (**d**) cumulative energy consumption; (**e**) emissions from MOA; and (**f**) emissions from SOA.

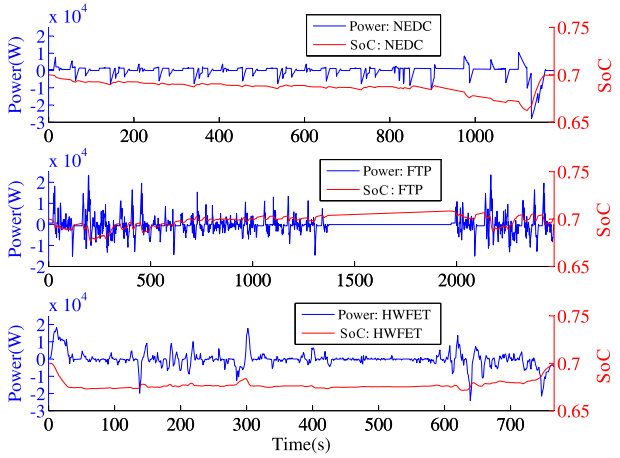

Figure 12. Battery output power and SoC under (**a**) NEDC, (**b**) FTP and (**c**) HWFET driving cycles.

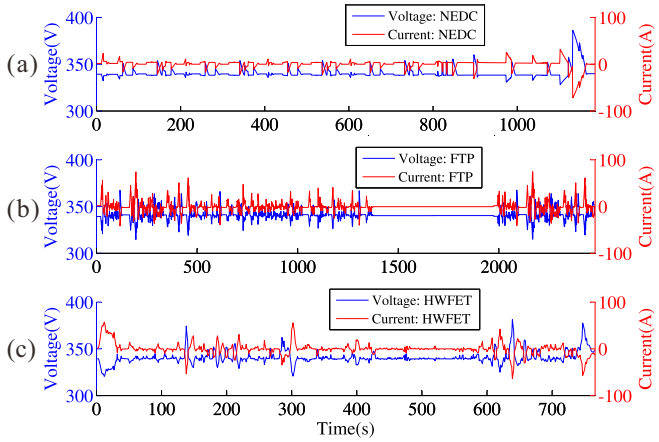

Figure 13. Battery voltage and current under (**a**) NEDC, (**b**) FTP and (**c**) HWFET driving cycles.

5.2. Experimental Results Analysis

The realtime fuel rates of the MOA and SOA are shown in Figures 9c–11c. It can be seen that there is no marked differences between the instantaneous fuel rate of the two approaches. The the cumulative energy consumption of the MOA and SOA for the three driving cycles are shown in Figures 9d–11d, respectively. The realtime emission rates of the two approaches are shown in Figures 9e–11e, respectively. As can be seen in these figures, the emission rates of the HC, CO and NO_x are relatively very high in the initial phase of each test cycle, this is mainly due to that the catalyst temperature is below the light-off temperature and the removal efficiency is very low. As experiment continues, the catalyst temperature as well as its removal efficiency increases gradually, and the emission rate of the pollutants decreases dramatically. Compared with Figures 9f–11f, it can be seen that Figures 9e–11e show significant reduction in the instantaneous emission rate of NO_x, HC and CO in most cases.

The quantitative results of total FC and HC, CO, NO_x production of the two approaches are presented in Table 2. In the third column of each metric, we compared the experimental results of the SOA with that of the proposed MOA by $\frac{R_{MOA}-R_{SOA}}{R_{SOA}} \times 100\%$, where R_{MOA} and R_{SOA} are the experimental results of the two approaches, respectively.

Table 2. Experimental results of the two approaches.

Cycles	FC (L/100 km)			HC (g/km)			CO (g/km)			NO_x (g/km)		
	SOA	MOA	%	SOA	MOA	%	SOA	MOA	%	SOA	MOA	%
NEDC	6.24	6.51	4.33	0.106	0.095	−10.38	1.077	0.994	−7.71	0.094	0.079	−15.96
FTP	6.91	7.16	3.62	0.116	0.106	−8.62	1.089	1.038	−4.68	0.118	0.095	−19.49
HWFET	4.90	5.06	3.27	0.069	0.059	−14.49	0.862	0.833	−3.36	0.076	0.066	−13.16
Average	6.02	6.24	3.74	0.097	0.087	−11.16	1.009	0.955	−5.25	0.096	0.080	−16.20

It can be seen from Table 2 that for all of the three driving cycles, the three air pollutants of the MOA are decreased to different extent compared with that of the SOA, at the sacrifice of a slight increase in FC (3.74% average). Furthermore, the NO_x emissions of the proposed MOA are significantly decreased (average 16.2%), while the other emissions (HC and CO) are slightly decreased (average 11.16% for HC and 5.25% for CO). This is due to that the weighting factors are set to $\omega_2 = 0.2$, $\omega_3 = 0.1$ and $\omega_4 = 0.3$, and the main aim of the MOM is to improve the NO_x emissions. The results of the three driving cycles show that the emissions reduction rates are positively correlated with the weighting factors. However, for different driving cycles, the emissions reduction rates are different, such as the CO reduction rate for NEDC is −7.71% while for HWFET driving cycle, it is only −3.36%. These indicate that the proposed APU operating point multi-objective optimization

method can effectively reduce the HC, CO and NO_x emissions at the expense of a slight drop in fuel efficiency, and the emissions reduction rates are positively correlated with the predefined weighting factors and determined by the specific driving cycle.

6. Conclusions

The locus of maximum fuel efficiency on the speed-torque map of an ICE does not necessarily corresponding to the loci of optimum emissions and there is a definite tradeoff between high fuel efficiency and low emissions. In order to balance the potentially conflicting goals of FC and fuel emissions reduction in the choice of operating point, the APU operating point multi-objective optimization model is proposed in this paper.

The proposed APU operating point multi-objective optimization model is solved by MOPSO algorithm and weighted metric decision making method and the optimization results are validated in bench experiments over three typically driving cycles. The experimental results show that compared with the traditional SOA, the results of the proposed MOA show significant improvements in the performance of emissions for all of the three driving cycles at the expense of a slight drop in fuel efficiency. In the face of growing air pollution, compared with the traditional APU operating point optimization approach which focuses only on the fuel efficiency and shows little sensitivity to the subtle emissions tradeoffs, the proposed approach opens a new way for the development of APU control strategy, especially in China, where the air quality is almost intolerable. The performance of the proposed approach under different combinations of weighting factors, as well as under other multi-objective optimization approaches, are important topics that requires further research.

Acknowledgments: The authors would like to thank the editors and reviewers for their corrections and helpful suggestions.

Author Contributions: Yongpeng Shen conceived the proposed APU operating point multi-objective optimization model, designed the experiments and drafted the manuscript; Zhendong He analyzed the experimental data and revised the full manuscript; Dongqi Liu and Binjie Xu performed the experiments.

Conflicts of Interest: The authors declare no conflict of interest.

References

1. Fiengo, G.; Glielmo, L.; Vasca, F. Control of auxiliary power unit for hybrid electric vehicles. *IEEE Trans. Control Syst. Technol.* **2007**, *15*, 1122–1130.
2. Castel-Branco, A.P.; Ribau, J.P.; Silva, C.M. Taxi fleet renewal in cities with improved hybrid powertrains: Life cycle and sensitivity analysis in Lisbon case study. *Energies* **2015**, *8*, 9509–9540.
3. Trovao, J.P.F.; Santos, V.D.N.; Antunes, C.H.; Pereirinha, P.G.; Jorge, H.M. A Real-time energy management architecture for multisource electric vehicles. *IEEE Trans. Ind. Electron.* **2015**, *62*, 3223–3233.
4. Hu, X.; Jiang, J.; Egardt, B.; Cao, D. Advanced power-source integration in hybrid electric vehicles: Multi-criteria optimization approach. *IEEE Trans. Ind. Electron.* **2015**, *62*, 7847–7858.
5. Mapelli, F.L.; Tarsitano, D.; Mauri, M. Plug-in hybrid electric vehicle: Modeling, prototype realization, and inverter losses reduction analysis. *IEEE Trans. Ind. Electron.* **2010**, *57*, 598–607.
6. He, B.; Yang, M. Robust LPV control of diesel auxiliary power unit for series hybrid electric vehicles. *IEEE Trans. Power Electron.* **2006**, *21*, 791–798.
7. Gokasan, M.; Bogosyan, S.; Goering, D.J. Sliding mode based powertrain control for efficiency improvement in series hybrid-electric vehicles. *IEEE Trans. Power Electron.* **2006**, *21*, 779–790.
8. Konev, A.; Lezhnev, L.; Kolmanovsky, I. Control Strategy Optimization for a Series Hybrid Vehicle. *SAE Tech. Pap.* **2006**, doi:10.4271/2006-01-0663.
9. Peng, J.; Fan, H.; He, H.; Pan, D. A rule-based energy management strategy for a plug-in hybrid school bus based on a controller area network bus. *Energies* **2015**, *8*, 5122–5142.
10. Wang, X.; He, H.; Sun, F.; Sun, X.; Tang, H. Comparative study on different energy management strategies for plug-in hybrid electric vehicles. *Energies* **2013**, *6*, 5656–5675.
11. Salmasi, F.R. Control strategies for hybrid electric vehicles: Evolution, classification, comparison, and future trends. *IEEE Trans. Veh. Technol.* **2007**, *56*, 2393–2404.

12. Shankar, R.; Marco, J.; Assadian, F. The novel application of optimization and charge blended energy management control for component downsizing within a plug-in hybrid electric vehicle. *Energies* **2012**, *5*, 4892–4923.
13. Williamson, S.S.; Rathore, A.K.; Musavi, F. Industrial electronics for electric transportation: Current state-of-the-art and future challenges. *IEEE Trans. Ind. Electron.* **2015**, *62*, 3021–3032.
14. Wang, X.; He, H.; Sun, F.; Zhang, J. Application study on the dynamic programming algorithm for energy management of plug-in hybrid electric vehicles. *Energies* **2015**, *8*, 3225–3244.
15. Johnson, V.H.; Wipke, K.B.; Rausen, D.J. HEV Control Strategy for Real-Time Optimization of Fuel Economy And Emissions. *SAE Tech. Pap.* **2000**, doi:10.4271/2000-01-1543.
16. Ehsani, M.; Gao, Y.; Emadi, A. *Modern Electric, Hybrid Electric, and Fuel Cell Vehicles: Fundamentals, Theory, and Design*, 2nd ed.; CRC Press: New York, NY, USA, 2010.
17. Gao, J.; Sun, F.; He, H.; Zhu, G.G.; Strangas, E.G. A comparative study of supervisory control strategies for a series hybrid electric vehicle. In Proceedings of the IEEE Power and Energy Engineering Conference, Wuhan, China, 27–31 March 2009; pp. 1–7.
18. Barsali, S.; Miulli, C.; Possenti, A. A control strategy to minimize fuel consumption of series hybrid electric vehicles. *IEEE Trans. Energy Convers.* **2004**, *19*, 187–195.
19. Sezer, V.; Gokasan, M.; Bogosyan, S. A novel ECMS and combined cost map approach for high-efficiency series hybrid electric vehicles. *IEEE Trans. Veh. Technol.* **2011**, *60*, 3557–3570.
20. Yoo, H.; Sul, S.K.; Park, Y.; Jeong, J. System integration and power-flow management for a series hybrid electric vehicle using supercapacitors and batteries. *IEEE Trans. Ind. Appl.* **2008**, *44*, 108–114.
21. Li, Y.; Pedroni, N.; Zio, E. A Memetic Evolutionary Multi-Objective Optimization Method for Environmental Power Unit Commitment. *IEEE Trans. Power Syst.* **2013**, *28*, 2660–2669.
22. Goudos, S.; Gotsis, K.; Siakavara, K.; Vafiadis, E.; Sahalos, J. A Multi-objective approach to Subarrayed Linear Antenna Arrays Design Based on Memetic Differential Evolution. *IEEE Trans. Antennas Propag.* **2013**, *61*, 3042–3052.
23. Salinas, S.; Li, M.; Li, P. Multi-objective optimal energy consumption scheduling in smart grids. *IEEE Trans. Smart Grid* **2013**, *4*, 341–348.
24. Ashby, M. Multi-objective optimization in material design and selection. *Acta Mater.* **2000**, *48*, 359–369.
25. Xue, X.; Cheng, K.W.E.; Ng, T.W.; Cheung, N.C. Multi-objective optimization design of in-wheel switched reluctance motors in electric vehicles. *IEEE Trans. Ind. Electron.* **2010**, *57*, 2980–2987.
26. Maciel, R.S.; Rosa, M.; Miranda, V.; Padilha-Feltrin, A. Multi-objective evolutionary particle swarm optimization in the assessment of the impact of distributed generation. *Electr. Power Syst. Res.* **2012**, *89*, 100–108.
27. Pareto, V. *Cours D'economie Politique*; Librairie Droz: Geneva, Switzerland, 1964. (In Italian)
28. Zitzler, E.; Thiele, L. Multiobjective evolutionary algorithms: A comparative case study and the strength Pareto approach. *IEEE Trans. Evol. Comput.* **1999**, *3*, 257–271.
29. Deb, K.; Pratap, A.; Agarwal, S.; Meyarivan, T. A fast and elitist multiobjective genetic algorithm: NSGA-II. *IEEE Trans. Evol. Comput.* **2002**, *6*, 182–197.
30. Coello, C.A.C.; Pulido, G.T.; Lechuga, M.S. Handling multiple objectives with particle swarm optimization. *IEEE Trans. Evol. Comput.* **2004**, *8*, 256–279.
31. Zhang, Q.; Li, H. MOEA/D: A multiobjective evolutionary algorithm based on decomposition. *IEEE Trans. Evol. Comput.* **2007**, *11*, 712–731.
32. Kahraman, C.; Ruan, D.; Dogan, I. Fuzzy group decision-making for facility location selection. *Inf. Sci.* **2003**, *157*, 135–153.
33. Renaud, J.; Thibault, J.; Lanouette, R.; Kiss, L.N.; Zaras, K.; Fonteix, C. Comparison of two multicriteria decision aid methods: Net Flow and Rough Set Methods in a high yield pulping process. *Eur. J. Oper. Res.* **2007**, *177*, 1418–1432.
34. Coello, C.A.C.; Lamont, G.B.; Van Veldhuisen, D.A. *Evolutionary Algorithms for Solving Multi-Objective Problems*; Springer: New York, NY, USA, 2007.
35. Kennedy, J.; Eberhart, R. Particle swarm optimization. In Proceedings of the IEEE International Conference on Neural Networks, Perth, Australia, 27 November–1 December, 1995; pp. 1942–1948.